ELSEVIER

Nuclear Instruments and Methods in Physics Research A 466 (2001) 202–208

NUCLEAR INSTRUMENTS & METHODS IN PHYSICS RESEARCH Section A

www.elsevier.nl/locate/nima

Characterisation of a single photon counting pixel detector

M.S. Passmore[a,*], R. Bates[a], K. Mathieson[a], V. O'Shea[a], M. Rahman[a], P. Seller[b], K.M. Smith[a]

[a] *Department of Physics and Astronomy, University of Glasgow, Glasgow, Scotland, UK G12 8QQ*
[b] *Rutherford Appleton Laboratory, Chilton, OXON, UK OX11 0QX*

Abstract

The Large Area Detector is a photon counting detector based on pixel readout ASICs with 64×64 arrays of 150 μm square pixels bump bonded to a 300 μm thick Si detector. It is designed for X-ray diffraction studies and is capable of up to 1 MHz count rate per pixel. A prototype has been tested at the synchrotron radiation source in Daresbury in a 19.5 keV X-ray beam. This paper focuses on the spatial resolution and noise performance. The calculation of modulation transfer functions leads to analytical formulae allowing the determination of the theoretical spatial resolution.

PACS: 07.85.Qe; 07.85.Fv; 07.85.Yk

Keywords: Detector; X-ray; MTF; Spatial resolution; Poisson noise; Photon-counting; Pixel

1. Introduction

The spatial resolution is an important parameter of any imaging detector. For state-of-the art pixel detectors the pixel size dominates the spatial resolution, which is conventionally measured in terms of the line spread function (LSF) or the modulation transfer function (MTF) [1,2]. For this work, the spatial resolution is defined as the number of line pairs per mm at an MTF value of 0.3.

Experimentally the LSF is acquired by taking an image of a narrow slit, i.e., the slit width should be several times smaller than the pixel size. For square pixel detectors, the LSF will have a significant dependence on the orientation of the slit. The spatial resolution is strongly dependent on the pixel size and shows a slight variation with the slope of the slit. Section 3 below describes a calculation of the resolution from the pixel geometry which results in an analytical formula giving the resolution of any square pixel detector. It also shows that the spatial resolution is dependent on the area of the pixel, not its geometric shape.

For comparison with the theory, spatial resolution measurements were performed with the Large Area Detector (LAD1) system, described in Section 2. The LAD1 is a state-of-the art single photon counting pixel detector. Since the theory is based purely on geometry, it is valid for any pixel detector (with symmetrical pixels).

Another performance defining parameter is the image noise, which is a measure of the variation in

*Corresponding author. Tel.: +44-141-330-6435; fax: +44-141-330-5881.

E-mail address: s.passmore@physics.gla.ac.uk (M.S. Passmore).

0168-9002/01/$ - see front matter
PII: S0168-9002(01)00846-4

the response of the pixels and indicates how reproducible and reliable an image is. It can be measured by taking successive images under identical conditions and measuring the spread in the response. For any imaging system this is limited by "photon statistics" (i.e., Poisson noise).

2. The LAD1

The LAD1 uses a 64×64 array read-out chip. The 300 μm thick Si detector has 150 μm square pixels. Each read-out cell contains a pre-amplifier, shaper, comparator and 15 bit pseudo-random counter. The comparator threshold is adjustable between 2 and 25 keV. Each pixel can take a count rate of 1 MHz. The data are shifted out at 10 MHz with 16 parallel channels, giving an acquisition time of 384 μs per image. Details of the system are given in Refs. [3,4].

3. Calculation of the MTF

For noncircular pixels, the LSF will depend on the angle at which the slit is placed across the detector. The x-axis of the LSF is given by the distance to the centre of the pixel. The amplitude or y-axis is proportional to the length of the slit within the pixel boundary. For square pixels this is shown in Fig. 1.

Before looking at different pixel sizes, the influence of the angle at which the slit is placed

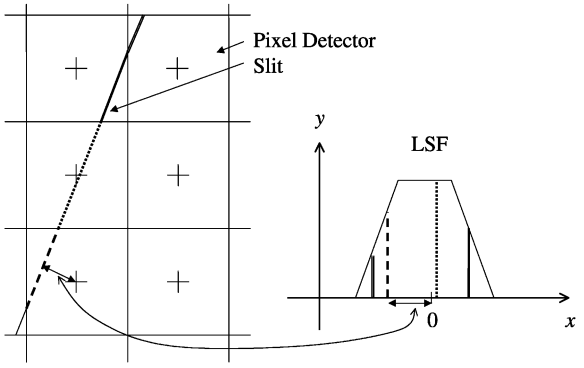

Fig. 1. The figure shows the method used for calculating the LSF in the case of square pixels.

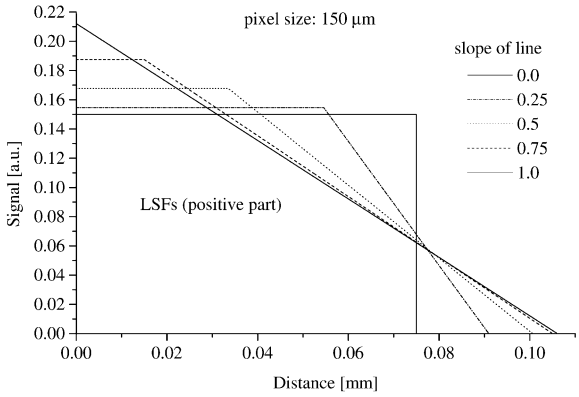

Fig. 2. Theoretically calculated LSFs for different orientations of the slit.

across the detector will be discussed. The theoretical LSFs and MTFs of a pixel detector with 150 μm square pixels are shown for different alignments of the slit. Taking the row number as x-axis and the column number as y-axis, the orientation of the slit is given by $y = mx + d$, where m is the slope of the slit, d the offset in pixels and $0 \leqslant m \leqslant 1$ will take all possible orientations into account, due to the symmetry of the detector. The calculated LSFs for some values of m are shown in Fig. 2.

Due to the symmetry of the LSF it is sufficient to consider the positive part only. Accordingly only the positive halves of the LSFs are shown in Fig. 2. The corresponding MTFs shown in Fig. 3 were calculated according to the formula

$$\mathrm{MTF}(z) = \int_0^\infty \mathrm{LSF}(x) \cos(2\pi x z)\, \mathrm{d}x, \qquad (1)$$

where z is the spatial frequency in line pair/mm. A value of '0' in the MTF corresponds to the average intensity, values between '0' and '−1' correspond to intensities between the mean and zero and are physically reasonable.

The oscillations seen in Fig. 3 are due to the LSF extending into the next period of the cosine (neighbouring line pair), which gives rise to interference patterns with the actual signal in that line pair. So the oscillations are caused by integrating over more than one line pair (one period in the cosine) and can be eliminated by simply reducing the integral boundary to $1/2z$

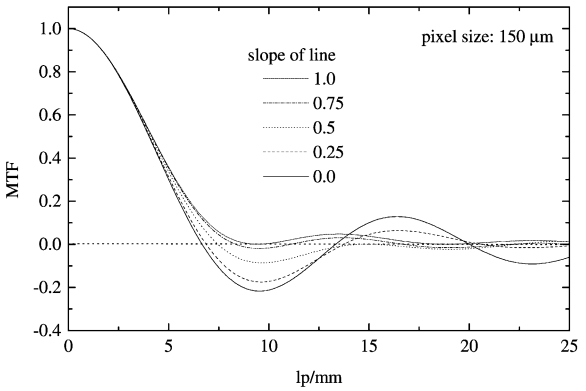

Fig. 3. Corresponding MTFs to the above shown LSFs.

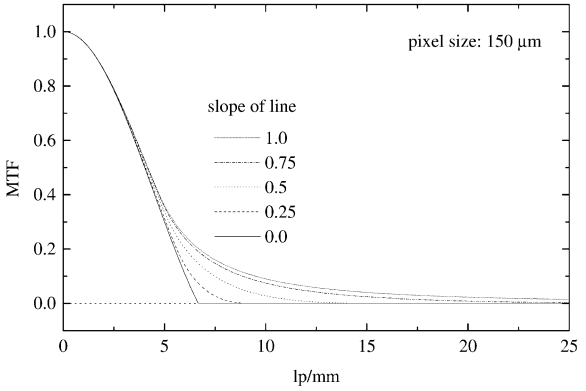

Fig. 4. MTFs calculated by integrating over one period only. This eliminates the interference and therefore the oscillations.

instead of ∞:

$$\mathrm{MTF}(z) = \int_0^{1/2z} \mathrm{LSF}(x)\cos(2\pi xz)\,\mathrm{d}x. \qquad (2)$$

Calculating the MTFs from the same LSFs as before (Fig. 2) leads to the curves shown in Fig. 4. The MTFs in Fig. 4 correspond to a single period instead of an infinite number of line pairs.

The MTF has a noticeable dependence on the orientation of the slit. When evaluating the number of line pairs per mm (lp/mm) a system can resolve, this number conventionally corresponds to an MTF of 0.3. At this MTF value (as shown in Figs. 3 and 4), the variation with the orientation of the slit is below 5% of the mean value. For further discussion, the spatial resolution is defined as the number of lp/mm at an MTF value of 0.3. With this definition, a comparison of different pixel sizes and geometries can be performed. For square pixels and a slope of 0.5 the resolution as a function of the pixel size is plotted in Fig. 5.

For any given slope the spatial resolution at an MTF value of 0.3 is given by

$$\text{Spatial resolution (lp/mm)} = \frac{k(\text{slope})}{\text{pixel size (mm)}} \qquad (3)$$

where k(slope) is a constant, dependent only on the slope of the line and from the pixel symmetry it is sufficient to consider values of slope between '0' and '1'. k(slope) is plotted in Fig. 6, the two curves representing the different limits of integration.

In order to obtain a simple formula for calculating the spatial resolution of any pixel size at a given slope, an analytical expression for k(slope) is convenient. The curves in Fig. 6 are well described by a function of the form

$$f(\text{slope}) = a\mathrm{e}^{-b((\ln|\text{slope}|)^2)^c} + d \qquad (4)$$

which has the desired symmetry properties. The choice of function is arbitrary, the only requirement is that it must be a good representation of k(slope). The fit to the data for infinite integration boundaries is shown in Fig. 7. The maximum deviation of k(slope) from the calculated data

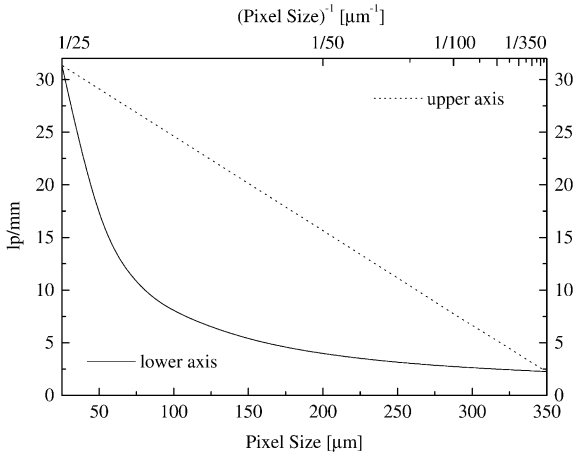

Fig. 5. The maximum theoretically achievable resolution, for a slope of 0.5, is plotted against the size of a square pixel. The resolution is inverse proportional to the pixel size, shown as the dotted line.

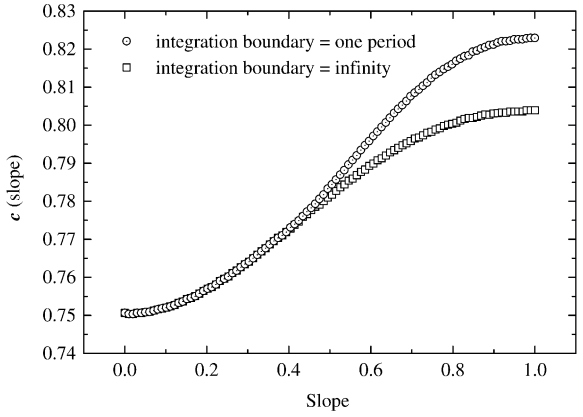

Fig. 6. k(slope) is plotted for values between '0' and '1' for integration boundaries of one period and infinity.

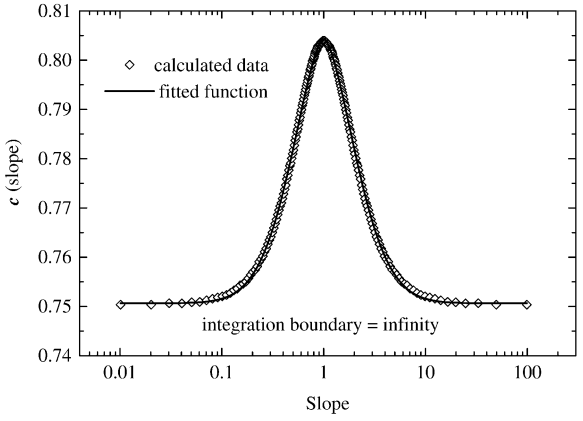

Fig. 7. Calculated data points and fitted k(slope) function. The x-axis is logarithmic to show a wider range of slope values.

Table 1
Values of the parameters determined for k(slope)

Integration boundary	a	b	c	d
Infinity	0.0532	1.037	0.852	0.7512
One period	0.0725	1.397	0.787	0.7519

points is 0.1%, (0.2% in the case of integrating over one period).

The values of $a-d$ are given in Table 1. The number of digits are chosen to have the same significance on the result while keeping the accuracy given by the fit of k(slope).

Finally, a theoretical limit for the spatial resolution as a function of the pixel size and slope of the line can be calculated from

$$\text{Spatial-Res.}_{\infty}\ (\text{lp/mm}) = \frac{0.0532\text{e}^{-(1.037(\ln|\text{slope}|)^2)^{0.852}} + 0.7512}{\text{pixel size (mm)}} \quad (5)$$

$$\text{Spatial-Res.}_{\text{one p}}\ (\text{lp/mm}) = \frac{0.0725\text{e}^{-(1.397(\ln|\text{slope}|)^2)^{0.787}} + 0.7519}{\text{pixel size (mm)}} \quad (6)$$

for integration boundaries of infinity and one period, respectively. The inaccuracy of the fit dominates the errors, the formulae agreeing with calculated values to $<0.2\%$.

3.1. Pixel geometry

Although so far only the square pixel geometry has been considered, in principle any geometry can be used. The next most common is the hexagonal or honeycomb structure. To draw a comparison between the theoretically achievable spatial resolution of different geometries, it is assumed that the areas of the pixels are the same. Instead of an hexagonal structure an evaluation was made of a circular structure as this has the highest symmetry and no slope dependence. The MTF of a circular and square pixel is shown in Fig. 8. For the latter, the slope of the line is 0.5. The dependence of the square pixel MTFs on the slope is far greater than the difference seen between the MTFs in Fig. 8. It is concluded that there will be no significant difference in the spatial resolution between a square and hexagonal pixel geometry.

4. Measurement of the LSF

The measurements were made with the LAD1 system. Images of a slit were taken in a 19.5 keV X-ray beam at the Daresbury SRS. A direct measurement of the slit width was not feasible. An estimate is possible by comparing the measured number of counts with and without the slit in the beam. Without the slit, the number of counts was

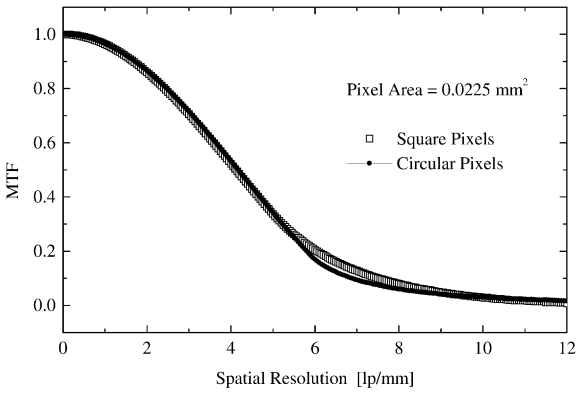

Fig. 8. MTF of a circular and square pixel geometry with the same area. There is no significant difference.

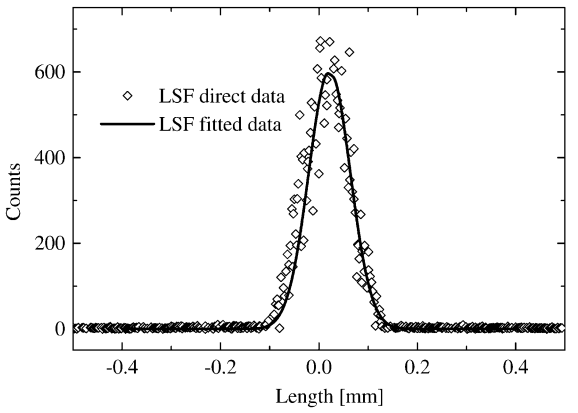

Fig. 10. Experimental LSF with the fitted function.

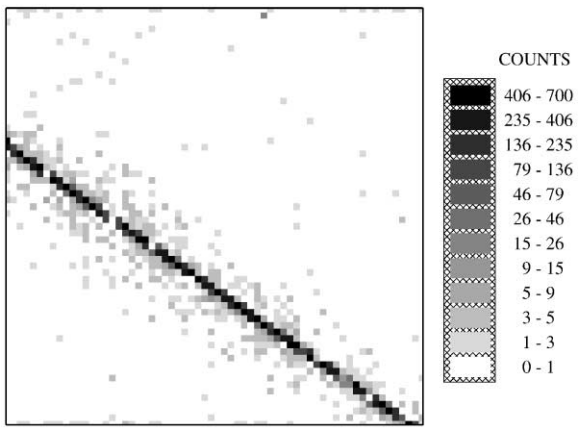

Fig. 9. Image of a slit used for the calculation of the MTF. The grey scale corresponds to the log(counts) to make the low counts in pixels visible.

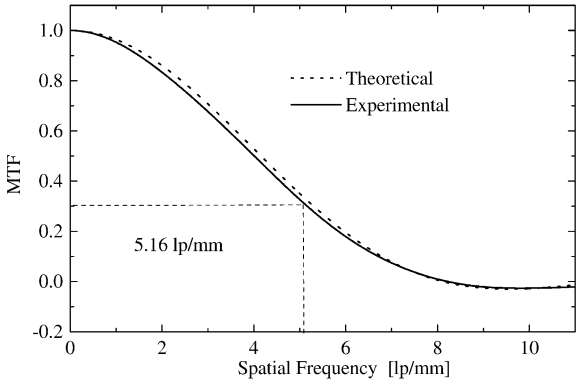

Fig. 11. Experimental and theoretical MTFs for integration boundaries of infinity.

approximately 5 times higher than with the slit, therefore the slit leaves about a fifth of the pixel area exposed, i.e., the width of the slit is about a fifth of the pixel size or 30 μm.

To reduce aliasing errors the slit was positioned at a steep angle (slope = 0.68) with respect to rows and columns of the pixel array. An image of the slit is shown in Fig. 9, and the LSF extracted from these data is shown in Fig. 10.

The MTFs calculated from the LSF are plotted with the theoretical MTFs in Figs. 11 and 12 for integration boundaries of infinity and one period, respectively.

From Figs. 11 and 12, it is seen that the LAD1 has a spatial resolution of about 5.2 lp/mm. In Fig. 12, the influence of the Nyquist frequency can be observed for spatial frequencies above about 5.5 lp/mm. The experimental MTFs are slightly lower than the theoretical curves, the spatial resolution is calculated to be 5.30 lp/mm (experiment: 5.16 lp/mm) and 5.37 lp/mm (experiment: 5.27 lp/mm) for integration boundaries of infinity and one period, respectively. Effects which could lead to a broadening of the LSF are charge sharing and the finite width of the slit. Double hits caused by charge sharing would significantly increase the width of the LSF since any hit is weighted equally and not according to the charge leading to the event.

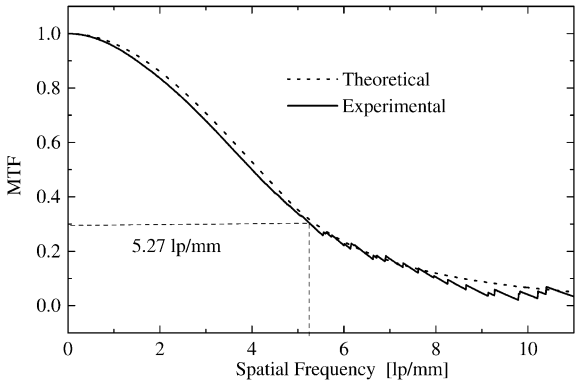

Fig. 12. Experimental and theoretical MTFs for integration boundaries of one period.

5. Image noise

In the context of imaging detectors the term "noise" is used as a measure of the variation in the response of a pixel to several identical exposures.

For a photon counting system, this noise is due to a variation in the number of counts recorded by the pixel, resulting from the Poisson statistics of the photon source [5]. The Poisson distribution is characterised by a variance equal to the mean value, so that the uncertainty on a number of counts is equal to the square root of the number of counts. This is referred to as Poisson noise ("photon statistics") and is of a lower theoretical limit to the noise achievable with any detector.

Since the detection involves several processes it is useful to consider the influence which each of them has on the noise.

The following points are considered:

(i) Absorption properties of the detector.
(ii) The threshold.
(iii) Noise events.
(iv) Timing errors.

The absorption properties and the threshold can both lower the mean number of counts recorded, but will not affect Poisson statistics.

If noise counts are independent and random, the probability of getting a noise count in a given time interval will be constant and Poisson statistics apply. Since combinations of Poisson distributions are again Poisson distributed the statistics do not change.

While none of the above mentioned effects change the Poisson statistics, one possible error may occur when taking the data from successive images. If the error in the exposure time dominates the overall statistical error, a linear dependence of the noise with dose is observed.

The mean number of experimentally observed counts μ will be $\mu = rt$ where t is the exposure time and r is the mean rate of the source reduced by any losses. If t has a Gaussian timing error Δt then the probability distribution $f(n,t)$ for the number of counts is

$$f(n,t) = \frac{(rt)^n}{n!}\mathrm{e}^{-rt}\frac{1}{\sqrt{2\pi}\Delta t}\mathrm{e}^{-(t-t_0)^2/2\Delta t^2}, \tag{7}$$

where t_0 is the mean exposure time.

The expectation value for the number of counts n is

$$\langle n\rangle = \int \mathrm{d}t \sum_n n\frac{(rt)^n}{n!}\mathrm{e}^{-rt}\frac{1}{\sqrt{2\pi}\Delta t}\mathrm{e}^{-(t-t_0)^2/2\Delta t^2} = rt_0. \tag{8}$$

The second moment $\langle n^2\rangle$ is

$$\langle n^2\rangle = \int \mathrm{d}t \sum_n n^2\frac{(rt)^n}{n!}\mathrm{e}^{-rt}\frac{1}{\sqrt{2\pi}\Delta t}\mathrm{e}^{-(t-t_0)^2/2\Delta t^2} = rt_0 + r^2t_0^2 + r^2\Delta t^2. \tag{9}$$

The variance is

$$\mathrm{var}(n) = \langle n^2\rangle - \langle n\rangle^2 = rt_0 + r^2\Delta t^2. \tag{10}$$

So at a low rate and accurate timing Poisson noise is observed, for high rate and inaccurate timing the standard deviation on the number of counts increases linearly with increasing rate.

Approximating the timing error with a Gaussian assumes that the negative part of the integral ($t<0$) can be neglected. This is valid for $t/\Delta t \gtrapprox 3$.

6. Measurement of the image noise

One hundred images of a slit were taken under similar conditions. The nominal exposure time was 20 ms; the X-ray source was monochromatic with an energy of 19.5 keV (SRS). For each pixel, the

mean and standard deviation were calculated. The image of a slit, shown in Fig. 13, includes pixels with different numbers of counts, which is useful for investigating the image noise.

For all pixels registering more than 5 counts, the mean number of counts is plotted against the variance in Fig. 14. A linear fit to the data gives a slope of 0.968 ± 0.019.

The pixels denoted as P1–P3 show a non-Poisson noise behaviour. Since they are outside the illuminated area, (see Fig. 13), they do not receive any photons and are assumed to be "noisy".

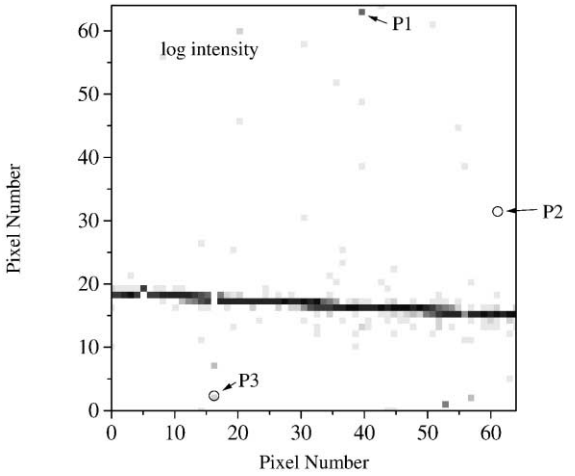

Fig. 13. Image of the slit used for investigating the image noise. The highlighted pixels are noisy and show a non-Poisson noise behaviour.

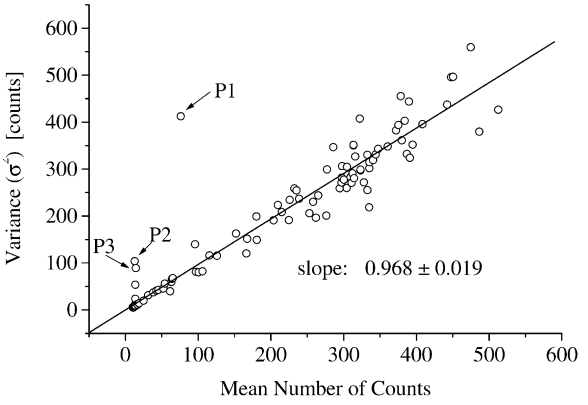

Fig. 14. The variance is plotted against the mean number of counts. According to Poisson statistics this should give a line with a slope of one.

7. Conclusions

For pixel detectors, the theoretical spatial resolution can be calculated. Measurements performed with the LAD1 deviate by about 2% from the calculated values. The achieved spatial resolution with the LAD1 system is 5.2 lp/mm. The image noise for photon counting detectors is expected to be given by Poisson statistics. This was confirmed using data obtained with the LAD1 system.

Acknowledgements

This work is funded through the Department of Trade and Industry Foresight initiative and is administered by PPARC under the IMPACT project. We thank the Daresbury support team and especially the station manager for their vital help at the SRS.

References

[1] C. Fröjdh, P. Nelvig, Phys. Med. XIV (Suppl. 2) (1998) 10.
[2] Modulation transfer function of screen film systems, International Commission on Radiation Units and Measurement, ICRU Report 41, 1986, http://www.ICRU.org
[3] P. Seller et al., Two approaches to hybrid X-ray pixel array readout, Detectors for Crystallography and Diffraction Studies at Synchrotron Sources, SPIE, Vol. 3774, July 1999.
[4] P. Seller et al., Nucl. Instr. and Meth. A 455 (2000) 715.
[5] R.J. Barlow, Statistics, Wiley, New York, 1989.